HHS Public Access

Author manuscript

Environ Sci Technol. Author manuscript; available in PMC 2015 November 13.

Published in final edited form as:

Environ Sci Technol. 2015 September 1; 49(17): 10642–10650. doi:10.1021/acs.est.5b01841.

Lipopolysaccharide Density and Structure Govern the Extent and Distance of Nanoparticle Interaction with Actual and Model Bacterial Outer Membranes

Kurt H. Jacobson[†,¶,○], **Ian L. Gunsolus**[‡,¶], **Thomas R. Kuech**[§], **Julianne M. Troiano**[||], **Eric S. Melby**[§], **Samuel E. Lohse**[⊥,◆], **Dehong Hu**[#], **William B. Chrisler**[#], **Catherine J. Murphy**[⊥], **Galya Orr**[#], **Franz M. Geiger**[||], **Christy L. Haynes**[‡,*], and **Joel A. Pedersen**[†,§,∇,*]

[†]Department of Civil and Environmental Engineering, University of Wisconsin, Madison, Wisconsin 53706, United States

[§]Environmental Chemistry and Technology Program, University of Wisconsin, Madison, Wisconsin 53706, United States

[∇]Department of Chemistry, University of Wisconsin, Madison, Wisconsin 53706, United States

[‡]Department of Chemistry, University of Minnesota, Minneapolis, Minnesota 55455, United States

[||]Department of Chemistry, Northwestern University, Evanston, Illinois 60208, United States

[⊥]Department of Chemistry, University of Illinois at Urbana–Champaign, Urbana, Illinois 61801, United States

[#]Environmental Molecular Sciences Laboratory, Pacific Northwest National Laboratory, Richland, Washington 99352, United States

Abstract

Design of nanomedicines and nanoparticle-based antimicrobial and antifouling formulations and assessment of the potential implications of nanoparticle release into the environment requires understanding nanoparticle interaction with bacterial surfaces. Here we demonstrate the electrostatically driven association of functionalized nanoparticles with lipopolysaccharides of Gram-negative bacterial outer membranes and find that lipopolysaccharide structure influences the extent and location of binding relative to the outer leaflet-solution interface. By manipulating the lipopolysaccharide content in *Shewanella oneidensis* outer membranes, we observed the electrostatically driven interaction of cationic gold nanoparticles with the lipopolysaccharide-containing leaflet. We probed this interaction by quartz crystal microbalance with dissipation

[*]Corresponding Authors: Phone: 608-263-4971; joelpedersen@wisc.edu. Phone: 612-626-1096, chaynes@umn.edu.
[○]K.H.J.: Department of Environmental Systems Science, ETH Zürich, Zürich, Switzerland.
[◆]S.E.L.: Department of Chemistry, Colorado Mesa University, Grand Junction, CO 81501.

[¶]Author Contributions

K.H.J and I.L.G. contributed equally to this work.

Notes

The authors declare no competing financial interest.

Supporting Information

The Supporting Information is available free of charge on the ACS Publications website at DOI: 10.1021/acs.est.5b01841. Lipid vesicle preparation and analysis methods, LPS molar mass analysis, harmonic-dependence analysis of QCM-D response, hyperspectral imaging analysis methods, and flow cytometry gating methods. (PDF)

monitoring (QCM-D) and second harmonic generation (SHG) using solid-supported lipopolysaccharide-containing bilayers. The association of cationic nanoparticles increased with lipopolysaccharide content, while no association of anionic nanoparticles was observed. The harmonic-dependence of QCM-D measurements suggested that a population of the cationic nanoparticles was held at a distance from the outer leaflet-solution interface of bilayers containing smooth lipopolysaccharides (those bearing a long *O*-polysaccharide). Additionally, smooth lipopolysaccharides held the bulk of the associated cationic particles outside of the interfacial zone probed by SHG. Our results demonstrate that positively charged nanoparticles are more likely to interact with Gram-negative bacteria than are negatively charged particles, and this interaction occurs primarily through lipopolysaccharides.

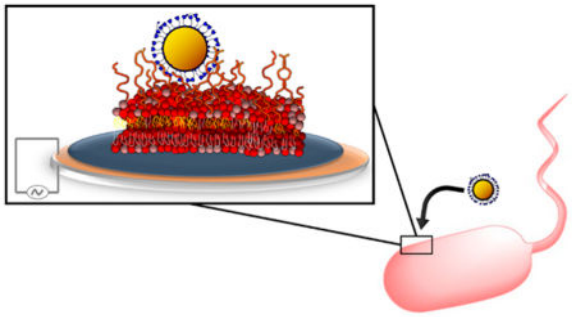

INTRODUCTION

In the early 2000s, products containing engineered nanomaterials (materials with at least one dimension <100 nm) began to enter commerce on a large scale.[1,2] Production and use of these materials has increased dramatically over the intervening years, leading to concerns about their potential environmental health and safety implications. Assessment of the potential risks associated with unintended release of engineered nanoparticles into the environment[3–5] is necessary to ensure the sustainable use of these materials, given their increasing integration into consumer products and the expectation that their contact with living organisms will induce biological responses.[6–8] Reliable risk assessment is currently hampered by the limited mechanistic insight into how nanoparticles interact with ecologically important organisms including bacteria, which represent an entry point into food chains. Current approaches for understanding interactions between nanoparticles and bacteria are typically indirect; many rely on monitoring changes in bacterial activity or survival in response to nanoparticle exposure, for example using quantitative structure–activity or high-throughput screening strategies.[9–11] Such approaches are favored mainly because the small size and biological complexity of bacteria remain barriers to direct characterization of nanomaterial-bacterial cell interactions. While insights have been derived from such indirect, correlative approaches, such as recent suggestions that cell-surface lipopolysaccharides (LPS) may be important in protecting Proteobacteria (a major group of Gram-negative bacteria) from the effects of cationic polystyrene and silver nanoparticles,[10,11] direct characterization of nanoparticle-bacterial cell interactions is needed to validate hypothesized mechanisms of interaction.

Here, we characterize nanoparticle interactions with bacteria directly at a level of molecular detail that is not currently attainable by monitoring microbial activity or survival. Moreover, we provide concrete evidence that LPS molecules protect Gram-negative bacteria from nanoparticles by forming a barrier to contact with and penetration of the outer membrane. The direct views of nanoparticle interactions with LPS achieved in this work show that a unique nanobiophysical interface controls nanomaterial interactions with Gram-negative bacteria, in which strain and growth condition-specific traits (i.e., LPS structure) influence the extent and nature (i.e., length-scale) of this interaction. A large variety of nanoparticle types may be explored. We focus here on electrostatics as a main driving force for nanoparticle–LPS interactions. Our experimental strategy was to evaluate the role of LPS and its structure in mediating interactions of cationic and anionic gold nanoparticles (AuNPs) with bacterial cell surfaces. We hypothesized that electrostatic interactions contribute strongly to nanoparticle interaction with LPS. To test our hypothesis, we used 4 nm-diameter AuNPs functionalized with mercaptopropane ligands terminated with either cationic or anionic moieties to probe the influence of nanoparticle charge on interactions with LPS in both live bacterial cells and solid-supported lipid bilayers.

MATERIALS AND METHODS

Gold Nanoparticle Preparation and Characterization

Gold nanoparticles (primary particle diameter = 4.0 ± 0.5 nm) were prepared[12] by a modified Brust procedure and functionalized with either 3-mercaptopropionic acid (MPA) or 3-mercaptopropyl amine ($MPNH_2$). These were chosen as model nanomaterials to investigate nanoparticle–LPS interactions due to their high chemical stability and well-controlled size, shape, and surface functionalization. Except where noted otherwise, experiments with AuNPs were conducted at a 12.8 nM number concentration in 0.002 M HEPES (pH 7.4) and 0.025 M NaCl.

Nanoparticle hydrodynamic diameter (Figure 1a) and electrophoretic mobility (Figure 1b) were measured by dynamic light scattering (DLS) and laser Doppler microelectrophoresis, respectively, as a function of solution ionic strength, *I*, using a Malvern ZetaSizer Nano ZS (Worcestershire, UK). Dynamic light scattering and electrophoretic mobility measurements were made 10 min after dilution of particle suspensions into solutions of the desired *I*. Both types of functionalized AuNPs formed larger aggregates as *I* increased. The hydrodynamic diameters for the MPA- and $MPNH_2$-AuNPs increased from ~50 nm at $I = 0.025$ M (Debye length, κ^{-1}, = 1.93 nm) to ~450 nm at $I = 0.100$ M ($\kappa^{-1} = 0.96$ nm) and were statistically indistinguishable from one another at each ionic strength ($p > 0.05$). The electrophoretic mobilities of the MPA- and $MPNH_2$-AuNPs were negative and positive, respectively, and did not vary with ionic strength over the range studied ($p < 0.05$).

Bacterial Culture

Shewanella oneidensis MR-1 (courtesy of Jeff Gralnick, University of Minnesota) was cultured in LB broth, achieving cell densities of ~1×10^9 cells·mL^{-1} at the stationary growth phase (24 h incubation at 30 °C with continuous shaking at 300 rpm).

Removal of LPS from Cells

Cells in LB broth were sedimented (10 min, 2000*g*), the supernatant was removed, and the cells were suspended in D-PBS to achieve a final cell density of 2×10^8 cells·mL^{-1}. Cell suspensions were split into two batches, and EDTA was added to one at a concentration of 0.005 M to remove a fraction of cell-surface LPS.[13] Both batches were then incubated with continuous shaking (10 min, 30 °C). Cells were sedimented by centrifugation (10 min, 2000*g*), the supernatant was removed and replaced with buffer (0.002 M HEPES, pH 7.4, I = 0.025 M), and the cells were resuspended. Three aliquots from each cell sample were removed and lyophilized, and their dry masses were recorded. The lyophilized cells were dissolved in 0.2 N H_2SO_4, and their LPS content was determined using the method described by Karkhanis et al.[14] (see the Supporting Information for details).

Nanoparticle–Cell Attachment Experiments

Following EDTA treatment and redispersal in buffer (*vide supra*), cells were mixed with AuNPs (12.8 nM number density) and incubated with continuous mixing (10 min, room temperature). Cells were then mixed 1:1 with 3.34 mM SYTO 9 (Life Technologies Kit L7012) and incubated 15 min prior to analysis by flow cytometry. Cells associated with AuNPs were identified via a combination of nucleic acid staining with SYTO 9 (to identify cells) and orthogonal (side) light scattering intensity detection (to identify nanoparticles) using a flow cytometer (Becton Dickenson LSRII SORP equipped with a 20 mW, 488 nm laser). Cells were then sorted into populations with and without associated AuNPs using a FACSAriaIIU cell sorter. Gating parameters for cell sorting are described in the Supporting Information.

After sorting, we acquired dark-field images of cell populations that were positive or negative for AuNPs with an Olympus BX43 microscope modified with a high signal-to-noise dark-field condenser unit (CytoViva, Auburn, AL). Hyperspectral images were acquired in the same field of view using the CytoViva hyperspectral imaging system consisting of a spectrophotometer (Specim) and spectrophotometer-integrated CCD (pco.pixelfly). Data were analyzed using the Spectral Angle Mapping feature of ENVI 4.8 software (Exelis Visual Information Solutions).

Nanoparticle-Bilayer Attachment Experiments

Unilamellar vesicles composed of 1-palmitoyl-2-oleoyl-*sn*-glycero-3-phosphocholine (POPC) or POPC with varying amounts of smooth or rough LPS were prepared and their hydrodynamic sizes, electrophoretic mobilities, and LPS contents[14] were determined as described in the Supporting Information. Solid-supported lipid bilayers were formed on SiO_2-coated QCM-D sensors via surface-mediated fusion of POPC or LPS-containing POPC vesicles[15] (Figure S4; see Supporting Information for details). The QCM-D instrument used was a Q-Sense E4 instrument (Biolin Scientific, Göteborg, Sweden) containing four sensors mounted in temperature-controlled, liquid flow cells. The fundamental frequency (f_1) of the sensors was 4.96 MHz. Except where noted otherwise, data are reported for the fifth harmonic (~25 MHz.).

Nanoparticle attachment experiments were commenced by pumping AuNP suspensions (12.8 nM number concentration; 0.002 M HEPES, pH 7.4, ionic strength adjusted with NaCl) over the supported lipid bilayers until the Δf and ΔD signals stabilized.[16] Nanoparticle-free buffer was then pumped through the flow cells to measure the detachment of nanoparticles from the POPC or POPC/LPS bilayers. Final areal mass density of lipid bilayers with and without associated AuNPs were estimated using the Sauerbrey equation[17,18] or Kelvin–Voight viscoelastic modeling[19] (Tables S1 and S3). For details, see the Supporting Information.

Second Harmonic Generation

Second harmonic generation (SHG) experiments were performed using a regeneratively amplified Ti:sapphire laser system (Hurricane, Spectra-Physics, 1 kHz repetition rate, 120 fs pulses) pumping an optical parametric amplifier (OPA-CF, Spectra-Physics) tuned to a fundamental wavelength between 610 and 615 nm as previously described[20–23] and further detailed in the Supporting Information. The *p*-polarized beam was focused onto the silica/buffer interface at which the bilayer was formed. The SHG signal was detected following our published procedures.[20–22] All SHG experiments were performed under static conditions.

Vesicles containing varying amounts of LPS (*vide supra*) were introduced into the cell and allowed to self-assemble into an LPS-containing lipid bilayer on the silica substrate. Various concentrations of AuNPs (10^{-14} to 10^{-8} M number concentration) in buffer were then introduced into the cell, and the SHG signal was monitored until it stabilized for at least 15 min. Nanoparticle-free buffer was introduced to the cell to assess the reversibility of the interaction of the particles with the bilayer.

RESULTS AND DISCUSSION

Nanoparticle-Cell Attachment

The bacterial cell envelope represents the critical contact point governing access of nanomaterials and their secondary products (e.g., reactive oxygen species, dissolved ions) to the cell interior. The structure of the Gram-negative bacterial cell envelope is complex: the inner phospholipid cell membrane is encompassed by a thin peptidoglycan cell wall, which itself is bounded by an outer membrane.[24] The outer membrane is an asymmetric structure. The inner leaflet is composed of phospholipids, while a major portion of the outer leaflet consists of complex lipopolysaccharides (LPS), a class of glycolipids.[24] LPS covers approximately 75% of the outer membrane surface of some bacteria[25] and serves as an important hydrophilic barrier (with significantly higher hydration levels than phospholipid bilayers),[26] protecting Gram-negative bacteria from antimicrobial peptides, hydrophobic antibiotics, and surfactants such as bile salts.[24,27] A typical full-length, or “smooth” LPS molecule is composed of three distinct domains: Lipid A (four to seven acyl chains attached to two phosphorylated glucosamines)[28] anchoring the LPS molecule in the outer membrane bilayer; a core oligosaccharide composed of hexoses, heptoses, and 3-deoxy-D-mannooctulosonic acids;[29] and the *O*-polysaccharide, a variable-length repeating oligosaccharide chain containing up to 50 repeat units[30] (Figure S1). At pH values typical of

the environment, all three domains carry a net negative charge from phosphate groups (pK_a < 3), and glucuronic acid (pK_a < 3), galacturonic acid (pK_a < 4), and *N*-acetylneuraminic acid (pK_a 2.6) residues. Some bacteria exhibit shorter types of LPS, referred to as "rough" LPS, which contains Lipid A and at least part of the core oligosaccharide, but lacks the *O*-polysaccharide. Owing to the abundance of LPS at the interface of the cell envelope of Gram-negative bacteria with the extracellular environment, understanding the molecular nature of its interactions with engineered nanoparticles is critical for assessing the potential for disruption or penetration of the Gram-negative bacterial cellular envelope.

We examined the association of AuNPs with live Gramnegative bacterial cells (*Shewanella oneidensis* MR-1, hereafter denoted *Shewanella*) as a function of cell LPS content and nanoparticle surface charge using a combination of flow cytometry, dark-field microscopy, and hyperspectral imaging. *Shewanella* was selected in part because the cells of this species have only a sparse distribution of extracellular polymeric substances at their membrane,[31–33] meaning that LPS (and not polysaccharide components that form a capsule around some bacterial cells) form the interface between these cells and their extracellular environment. To test the hypothesis that LPS mediates nanoparticle interaction with Gram-negative bacteria, as suggested by recent high-throughput screening studies of *Escherichia coli* interactions with polystyrene and silver nanoparticles[10,11] and cytotoxicity studies,[34,35] we prepared LPS-depleted *Shewanella* cells. Brief treatment with EDTA[13,36] removed ~50% of cell LPS from the outer membrane (Figure S2), as determined by colorimetric measurement of 8-amino-3,8-dideoxy-D-*manno*-octulosonic acid (8-amino-2-keto-3-deoxy-D-manno-octonate, 8-aminoKdo),[14] a *Shewanella* species-specific aminated form of 3-deoxy-D-*manno*-octulosonic acid,[38,39] an essential component of LPS. Prior work on *E. coli* has demonstrated that this method removes LPS from the outer membrane without concomitant removal of proteins or leakage of cell contents.[13] The mechanism is suggested to involve chelation of divalent cations that cross-link LPS molecules through interaction with anionic sites such as phosphates,[26,36,37] releasing LPS into the solution.[13] Quantification of cell LPS content required that cells be sacrificed. Experiments with nanoparticles were performed on live cell populations with either native or depleted LPS content.

We exposed ~2×10^8 native and LPS-depleted *Shewanella* cells to cationic $MPNH_2$- or anionic MPA-functionalized AuNPs (10 min, 12.8 nM AuNP, I = 0.025 M, pH = 7.4; see Figure 1 for nanoparticle properties) and quantified the number of cells in each treatment associated with AuNPs by flow cytometry. Association of AuNPs with cells increases the light scattering cross-section. High-throughput analysis of the orthogonal light scattering intensity of individual cells was used to identify the presence of cell-associated AuNPs. Cells exhibiting light scattering above an intensity threshold, determined by control experiments with unexposed cells, were identified as positive for AuNPs. In this way, tens of thousands of cells were classified *in situ* as either negative or positive for cell-associated AuNPs. Cell analysis required no preparative steps after cell-nanoparticle exposure and did not disrupt cell-nanoparticle interaction because the measurement was made in solution. Putative AuNP-positive cells were isolated by fluorescence-activated cell sorting (FACS) and imaged by hyperspectral and dark-field microscopy to verify the presence of associated

AuNPs[40] and to establish FACS as an approach to discriminate between bacterial cells with and without associated AuNPs (Figure 2, Supporting Information Figures S3, and S5).

Removing ~50% of the cell LPS content decreased the number of cells with associated $MPNH_2$-AuNPs by ~70% (Figure 2). At the growth temperature used (30 °C), *Shewanella oneidensis* MR-1 produces only rough LPS (see Figure S6b); lower growth temperatures induce synthesis of smooth LPS.[32] Our results suggest that cationic nanoparticles bind preferentially to LPS, such that its removal decreases nanoparticle binding to the outer membrane. In contrast, anionic MPA-AuNPs did not appreciably associate with the cells, regardless of LPS content. Given the net negative charge of the Gram-negative bacterial cell surface at pH values typical of the environment,[41,42] this result suggests that electrostatic interactions control the association of nanoparticles with bacterial cells, as has been suggested in previous reports.[10,11,43,44]

We visually confirmed nanoparticle association with cells by dark-field microscopy and hyperspectral imaging. We separated bacterial cells with associated $MPNH_2$-AuNPs from the total cell population by FACS and acquired dark-field micrographs of them. The micrographs show single bacterial cells with cell-associated material producing high-intensity light scattering, indicative of AuNPs (Figure 2a). We confirmed the presence of AuNPs by comparing hyperspectral images of nanoparticle-associated bacterial cells with a spectral library of bacteria-free colloidal $MPNH_2$-AuNPs (Figure S3). Regions of the cell hyperspectral image matching the AuNP library are highlighted in the micrographs. This analysis confirmed that the observed cell-associated material was $MPNH_2$-AuNPs. In addition, dark-field micrographs of bacterial cells exposed to $MPNH_2$-AuNPs were acquired prior to cell sorting. These micrographs also show cell-associated material producing high-intensity light scattering, consistent with the previous analysis (Figure 2b).

Attachment of Cationic and Anionic Gold Nanoparticles to LPS-Containing Bilayers

To gain further molecular insight into the interaction of nanoparticles with lipopolysaccharides identified in the studies with live bacterial cells described above, we investigated the amount, reversibility, and length scale of $MPNH_2$- and MPA-AuNP association with LPS containing or lacking the *O*-polysaccharide using a quartz crystal microbalance with dissipation monitoring and second harmonic generation. The first step in these studies was to form LPS-containing lipid bilayers on QCM-D sensor surfaces. We prepared vesicles composed of POPC with variable amounts of rough or smooth LPS (see Figure 3 and the Supporting Information).[14] We then formed solid-supported LPS-containing bilayers on SiO_2-coated QCM-D sensors via fusion of LPS-containing POPC vesicles (Figure S4).[15]

We tested the hypothesis that electrostatics contributed strongly to nanoparticle interaction with LPS-containing bilayers by investigating the amount of cationic $MPNH_2$- and anionic MPA-AuNPs attaching to bilayers as a function of LPS content. These experiments were performed with 12.8 nM AuNPs in 0.002 M HEPES solution (pH 7.4) at I = 0.025 or 0.100 M. Figure 4a shows maximum frequency shifts measured by QCM-D following association of $MPNH_2$-AuNPs with lipid bilayers composed of pure POPC or POPC containing different amounts of smooth or rough LPS. The negative frequency shifts observed after

introduction of positively charged $MPNH_2$-AuNPs to all types of bilayers indicate nanoparticle association with the bilayers. The maximal frequency shifts and estimated areal mass densities for these systems are presented in Tables S2 and S3. Small amounts of $MPNH_2$-AuNP detachment were observed for most systems when they were rinsed with NP-free buffer (Figure S4). We did not detect interaction of the negatively charged MPA-AuNPs with any of the bilayers surveyed (mass detection limit for these systems was ~2 $ng \cdot cm^{-2}$).

In the experiments conducted at 0.025 M NaCl, association of cationic $MPNH_2$-AuNPs with lipid bilayers increased with the amount of rough or smooth LPS incorporated, and AuNP association was higher for smooth LPS-containing bilayers on a *per LPS molecule basis* (Figure 4a,b). Acoustic masses increased from 200 ± 10 $ng \cdot cm^{-2}$ for POPC bilayers to 320 ± 10 $ng \cdot cm^{-2}$ and 450 ± 10 $ng \cdot cm^{-2}$ for those containing 2.9 and 6.4 mol % rLPS (Table S3). For bilayers containing smooth LPS, acoustic masses were 280 ± 20 $ng \cdot cm^{-2}$ for bilayers containing 0.21 mol % sLPS and 330 ± 20 $ng \cdot cm^{-2}$ for those containing 0.46 mol % sLPS. These results point to the *O*-polysaccharide domain of smooth LPS molecules presenting many more potential binding sites for cationic nanoparticles to solution than the solvent-exposed portion of rough LPS molecules. Each rough LPS molecule used in our experiments contains two negative charges (phosphates associated with glucosamine residues in Lipid A).[47] In contrast, the smooth LPS molecules typically contain additional negatively charged moieties including additional phosphate groups and acidic sugars (e.g., glucuronic and galacturonic acids) in the outer core and *O*-polysaccharide domains,[48] which extend farther into solution than negatively charged moieties in rough LPS molecules. The higher abundance of negatively charged moieties in smooth LPS molecules relative to rough LPS molecules is evidenced in the electrophoretic mobility measurements of LPS-containing vesicles (Figure 3b). We note that the acyl chains of the ligands on the nanoparticles are three carbons long and terminate in a charged functional group. For bilayers composed solely of POPC, we expect the charged ligands bound to the nanoparticles would interact primarily with the phosphatidylcholine headgroup of these lipids.

Changes in QCM-D energy dissipation (ΔD) during $MPNH_2$-AuNP association differed between smooth and rough LPS-containing bilayers. The smooth LPS-containing bilayers exhibited larger increases in ΔD_5 (3.0 to 4.0 × 10^{-6}) than did POPC or rough LPS-containing bilayers (0.8 to 1.5 × 10^{-6}). This result indicates that $MPNH_2$-AuNPs interacting with smooth LPS-containing bilayers were less rigidly coupled to the vibrating resonator than those associated with POPC or rough LPS-containing bilayers.

At higher ionic strength (I = 0.100 M), the $MPNH_2$-AuNPs agglomerated (Figure 1a), and association with all bilayers decreased significantly relative to the experiments conducted at lower ionic strength (Figure 4a,b; Table S3). Association of $MPNH_2$-AuNPs with bilayers containing LPS (140 to 190 $ng \cdot cm^{-2}$) was higher than those composed of pure POPC (23 ± 4 $ng \cdot cm^{-2}$); however, the amounts associated with LPS-containing bilayers did not differ from each other ($p > 0.05$). These results indicate that smooth LPS induced higher nanoparticle association on a per molecule basis than did rough LPS. This result is consistent with the notion that smooth LPS, due to the presence of the *O*-polysaccharide,

presents a larger number of anionic sites for interaction with cationic AuNPs than does rough LPS on a per molecule basis.

Proximity of $MPNH_2$-AuNPs to the Phospholipid–Solution Interface

The harmonic-dependence of the QCM-D frequency and dissipation responses allows inference of the relative distance that AuNPs are held from the sensor-solution interface for the bilayers containing rough and smooth LPS. The penetration depth of the shear wave (δ) depends on the harmonic (n): $\delta = \eta_l/\pi n f_1 \rho_l)^{0.5}$, where η_l is liquid dynamic viscosity, f_1 is the fundamental frequency (4.96 MHz), and ρ_l is the liquid density.[19] Lower harmonics penetrate further into the medium overlying the sensor than do higher harmonics. We compared the dependence of changes in frequency ($\Delta f_n/n$) and dissipation (ΔD_n) on the harmonics monitored in experiments probing $MPNH_2$-AuNP association with smooth and rough LPS-containing bilayers (Figure 4c,d). Both $\Delta f_n/n$ and ΔD_n displayed pronounced harmonic-dependence for $MPNH_2$-AuNPs association with smooth LPS-containing bilayers; for the rough LPS-containing bilayer, $\Delta f_n/n$ and ΔD_n did not depend on the harmonic. While the penetration depth for all harmonics monitored (e.g., 145 and 76 nm for the third and 11th harmonics, respectively) exceeded the length of the LPS molecules (7–46 nm for smooth LPS),[49] signals for lower harmonics contain larger contributions from mass farther from the sensor surface than do higher harmonics. The more pronounced harmonic-dependence observed for $MPNH_2$-AuNP association with smooth compared to rough LPS-containing bilayers suggests that, in the former, at least some of the nanoparticle mass is held at a distance from the sensor surface (i.e., not directly in contact with the outer leaflet-solution interface). This is consistent with the notion that cationic particles interact with the *O*-polysaccharide domain of smooth LPS, because the *O*-polysaccharide presents anionic sites available for interaction with cationic nanoparticles that extend away from the bilayer surface.[50,51]

To gain further insight into the molecular origins of nanoparticle-bilayer interactions observed by QCM-D, we employed second harmonic generation (SHG). When excited with wavelengths near 600 nm, the SHG intensity near 300 nm increases when supported lipid bilayers are exposed to 4 nm AuNPs.[52] This nanoparticle-induced increase in intensity suggests resonance enhancement to the SHG signal upon AuNP adsorption to the bilayer-solution interface. Since the second-order nonlinear optical response is distance-dependent,[53,54] SHG can be used to probe the length scale of AuNP–bilayer interactions. This principle allowed us to evaluate the location of AuNPs associated with the bilayers relative to the outer leaflet-solution interface, which is the least symmetric, and thus the most SHG-active, region in our system.

Figure 5 shows the summary of our findings, while the Supporting Information contains the detailed results from our concentration-dependent SHG studies. Briefly, we find that exposing pure POPC bilayers to the $MPNH_2$-AuNPs under otherwise identical buffer and salt conditions increases the SHG signal intensity by more than 30%. Somewhat smaller SHG signal intensity gains were observed when the POPC bilayer contained 2.9 or 6.4 mol % rough LPS. In contrast, the SHG signal intensity either did not change or changed only slightly upon addition to the bilayers containing 0.21 or 0.46 mol% smooth LPS,

respectively. Exposure of LPS-containing bilayers to anionic MPA-AuNPs did not produce an increase in SHG signal intensity either (data not shown), consistent with the lack of interaction between the AuNPs and these bilayers demonstrated in the QCM-D experiments (*vide supra*).

Given that the QCM-D experiments described in the previous section show clear mass gains upon introduction of $MPNH_2$-AuNPs to bilayers containing both rough LPS and smooth LPS, we hypothesize that the lack of SHG signal intensity gains for the bilayers containing smooth LPS are due to the distance-dependence of the SHG process, as elaborated by Walker and co-workers.[53,54] Under this hypothesis, nanoparticles associated with LPS are held at a larger distance from the bilayer-solution interface than those bound to POPC. The resulting reduction in SHG resonance enhancement would then lead to smaller increases in SHG intensity induced by nanoparticle association with bilayers, which is indeed observed. This interpretation of the correlated SHG and QCM-D results is supported by reports from Walker and co-workers who used molecular tethers, or rulers, to place SHG-active chromophores at various distances from liquid/liquid interfaces and found longer distances to coincide with diminishing and finally vanishing SHG signal.[53,54] Quantitative distance measurements would, in principle, be possible by X-ray standing wave measurements[55] or by anchoring AuNPs to the LPS-containing bilayers using tethers of varying lengths, but such demanding experiments have their own caveats and exceed the scope of the current study. LPS structure also influenced changes in SHG intensity, evidenced by the smaller increase in SHG intensity upon nanoparticle binding to smooth LPS than rough LPS. Smooth LPS contains the *O*-polysaccharide absent in rough LPS and thus presents negatively charged binding sites for AuNPs at a larger distance from the bilayer–solution interface (outside the interfacial zone probed by SHG), resulting in lower intensity enhancement.

Effect of Nanoparticle–Bilayer Association on Lipid Structure

To investigate the potential effects of nanoparticle association with bilayers on the underlying lipid structure, super-resolution fluorescence micrographs of POPC bilayers with variable LPS content were acquired before and after addition of $MPNH_2$-AuNPs (Figure S9). TopFluor PC was used to construct fluorescent bilayers within glass-bottom dishes. Then $MPNH_2$-AuNPs were introduced under identical conditions to those used in QCM-D experiments (I = 0.025 M). The images show that nanoparticle addition to pure POPC bilayers and POPC bilayers containing smooth LPS alters lipid packing, evidenced by the formation of lipid clusters (bright regions due to locally increased fluorophore concentration). In contrast, the $MPNH_2$-AuNP introduction to POPC bilayers with rough LPS had no observable effect on lipid packing. This suggests that nanoparticle association with lipid bilayers, either through direct interaction with lipids or through interaction with LPS, may alter lipid packing. Evaluation of this hypothesis is the subject of ongoing work. We note, however, that the smooth LPS densities achieved in the supported lipid bilayers (0.21 to 0.46 mol %) are considerably lower than those occurring in bacteria that incorporate these molecules into their outer membranes. Our results suggest that bacterial outer membranes with higher smooth LPS densities would prevent contact of cationic nanoparticles with the bilayer.

Environmental Implications

The results of this study provide direct evidence for electrostatically driven association of cationic nanoparticles with the negatively charged polyssacharide portions of LPS molecules in the cell envelope of Gram-negative bacteria, supporting the hypothesis that LPS plays a critical role in mediating such nanoparticle–cellular interactions.[10,11,34,35] Acoustic and spectroscopic data from QCM-D and SHG measurements, respectively, on analogous supported lipid bilayers indicate that these interactions occur farther into solution (farther from the outer leaflet-solution interface) in bacteria that elaborate LPS including the long *O*-polysaccharide chain ("smooth" LPS) compared to those bearing short, "rough" LPS. Correlated super-resolution fluorescence imaging studies of these lipid bilayers demonstrate that interaction of cationic nanoparticles with the smooth LPS-containing bilayer impacts lipid packing. Electrostatic repulsion is expected to prevent most associations of anionic particles with membrane-bound LPS molecules both in whole bacterial cells and the model lipid bilayers.

The propensity of smooth LPS to hold bound nanoparticles at a distance from the bilayer-solution interface suggests a barrier function for the O-antigen that may protect bacteria from the effects of nanoparticles that require contact with the outer membrane bilayer to induce adverse effects. This insight leads to the expectation that bacteria bearing rough LPS may be more susceptible to the effects of intact nanoparticles than are those that produce smooth LPS, despite lower association of nanoparticles with the former. The efficacy of nanoparticles that exert their antimicrobial effect via dissolution (e.g., silver nanoparticles)[56] or production of reactive oxygen species (e.g., zinc oxide nanoparticles)[44,57] is expected to depend on the balance between higher association with smooth LPS (for cationic NPs) and the greater availability of sites for interaction or reaction on these molecules vis-à-vis rough LPS, to the extent that damage to LPS is not deleterious. The detailed characterization of nanoparticle interactions with bacterial cells and solid-supported lipid bilayers presented in this study demonstrates that LPS molecules mediate nanoparticle interactions with Gram-negative bacteria and provides molecular-level insight necessary to design engineered nanoparticles with reduced biological impact. Intriguingly, the LPS molecules that confer a barrier function to the outer membrane may also facilitate the entry of bacterial surface-bound nanoparticles into food chains.

Supplementary Material

Refer to Web version on PubMed Central for supplementary material.

Acknowledgments

This study was supported by the National Science Foundation (NSF) under the Center for Sustainable Nanotechnology (CHE-1240151). Part of the research was performed at EMSL, a Scientific User Facility sponsored by DOE-BER and located at PNNL. We thank the University of Minnesota's University Flow Cytometry Resource for flow cytometric analysis and FACS. I.L.G. gratefully acknowledges support through a National Institutes of Health Training for Future Biotechnology Development Grant (T32 GM008347) and a Minneapolis Torske Klubben Graduate Fellowship. J.M.T. gratefully acknowledges support through an NSF Graduate Research Fellowship. Partial funding for the QCM-D instrument was from NSF Grants DMR-0832760 and CBET-0826204. We thank Robert Hamers and Bill Hickey for helpful comments on the manuscript.

References

1. Sharifi S, Behzadi S, Laurent S, Forrest ML, Stroeve P, Mahmoudi M. Toxicity of Nanomaterials. Chem Soc Rev. 2012; 41:2323. [PubMed: 22170510]
2. Project on Emerging Nanotechnologies. Consumer Products Inventory; 2014.
3. Nowack B, Bucheli TD. Occurrence, Behavior and Effects of Nanoparticles in the Environment. Environ Pollut. 2007; 150:5–22. [PubMed: 17658673]
4. Moore MN. Do Nanoparticles Present Ecotoxicological Risks for the Health of the Aquatic Environment? Environ Int. 2006; 32:967–976. [PubMed: 16859745]
5. Mueller NC, Nowack B. Exposure Modeling of Engineered Nanoparticles in the Environment. Environ Sci Technol. 2008; 42:4447–4453. [PubMed: 18605569]
6. Ge Y, Priester JH, Van De Werfhorst LC, Schimel JP, Holden PA. Potential Mechanisms and Environmental Controls of TiO_2 Nanoparticle Effects on Soil Bacterial Communities. Environ Sci Technol. 2013; 47:14411–14417. [PubMed: 24256577]
7. Kumar N, Shah V, Walker VK. Perturbation of an Arctic Soil Microbial Community by Metal Nanoparticles. J Hazard Mater. 2011; 190:816–822. [PubMed: 21546158]
8. Collins D, Luxton T, Kumar N, Shah S, Walker VK, Shah V. Assessing the Impact of Copper and Zinc Oxide Nanoparticles on Soil: A Field Study. PLoS One. 2012; 7:42663.
9. Puzyn T, Rasulev B, Gajewicz A, Hu X, Dasari TP, Michalkova A, Hwang HM, Toropov A, Leszczynska D, Leszczynski J. Using Nano-QSAR to Predict the Cytotoxicity of Metal Oxide Nanoparticles. Nat Nanotechnol. 2011; 6:175–178. [PubMed: 21317892]
10. Ivask A, Suarez E, Patel T, Boren D, Ji Z, Holden P, Telesca D, Damoiseaux R, Bradley KA, Godwin H. Genome-Wide Bacterial Toxicity Screening Uncovers the Mechanisms of Toxicity of a Cationic Polystyrene Nanomaterial. Environ Sci Technol. 2012; 46:2398–2405. [PubMed: 22148163]
11. Ivask A, ElBadawy A, Kaweeteerawat C, Boren D, Fischer H, Ji Z, Chang CH, Liu R, Tolaymat T, Telesca D, et al. Toxicity Mechanisms in *Escherichia coli* Vary for Silver Nanoparticles and Differ from Ionic Silver. ACS Nano. 2014; 8:374–386. [PubMed: 24341736]
12. Lohse SE, Eller JR, Sivapalan ST, Plews MR, Murphy CJ. A Simple Millifluidic Benchtop Reactor System for the High-Throughput Synthesis and Functionalization of Gold Nanoparticles with Different Sizes and Shapes. ACS Nano. 2013; 7:4135–4150. [PubMed: 23634842]
13. Leive L. Release of Lipopolysaccharide by EDTA Treatment of *E. coli*. Biochem Biophys Res Commun. 1965; 21:290–296. [PubMed: 4159978]
14. Karkhanis YD, Zeltner JY, Jackson JJ, Carlo DJ. A New and Improved Microassay to Determine 2-Keto-3-Deoxyoctonate in Lipopolysaccharide of Gram-Negative Bacteria. Anal Biochem. 1978; 85:595–601. [PubMed: 646115]
15. Kaufmann S, Ilg K, Mashaghi A, Textor M, Priem B, Aebi M, Reimhult E. Supported Lipopolysaccharide Bilayers. Langmuir. 2012; 28:12199–12208. [PubMed: 22830310]
16. Jacobson KH, Kuech TR, Pedersen JA. Attachment of Pathogenic Prion Protein to Model Oxide Surfaces. Environ Sci Technol. 2013; 47:6925–6934. [PubMed: 23611152]
17. Sauerbrey G. Verwendung von Schwingquarzen Zur Wägung Dünner Schichten Und Zur Mikrowägung. Eur Phys J A. 1959; 155:206–222.
18. Reviakine I, Johannsmann D, Richter RP. Hearing What You Cannot See and Visualizing What You Hear: Interpreting Quartz Crystal Microbalance Data from Solvated Interfaces. Anal Chem. 2011; 83:8838–8848. [PubMed: 21939220]
19. Voinova MV, Rodahl M, Jonson M, Kasemo B. Viscoelastic Acoustic Response of Layered Polymer Films at Fluid-Solid Interfaces: Continuum Mechanics Approach. Phys Scr. 1999; 59:391–396.
20. Malin JN, Hayes PL, Geiger FM. Interactions of Ca, Zn, and Cd Ions at Buried Solid/Water Interfaces Studied by Second Harmonic Generation. J Phys Chem C. 2009; 113:2041–2052.
21. Hayes PL, Chen EH, Achtyl JL, Geiger FM. An Optical Voltmeter for Studying Cetyltrimethylammonium Interacting with Fused Silica/Aqueous Interfaces at High Ionic Strength. J Phys Chem A. 2009; 113:4269–4280. [PubMed: 19309099]

22. Hayes PL, Gibbs-Davis JM, Musorrafiti MJ, Mifflin AL, Scheidt KA, Geiger FM. Environmental Biogeochemistry Studied by Second-Harmonic Generation: A Look at the Agricultural Antibiotic Oxytetracycline. J Phys Chem C. 2007; 111:8796–8804.

23. Konek CT, Illg KD, Al-Abadleh HA, Voges AB, Yin G, Musorrafiti MJ, Schmidt CM, Geiger FM. Nonlinear Optical Studies of the Agricultural Antibiotic Morantel Interacting with Silica/Water Interfaces. J Am Chem Soc. 2005; 127:15771–15777. [PubMed: 16277520]

24. Silhavy TJ, Kahne D, Walker S. The Bacterial Cell Envelope. Cold Spring Harbor Perspect Biol. 2010; 2(5):a000414.

25. Le Brun AP, Clifton LA, Halbert CE, Lin B, Meron M, Holden PJ, Lakey JH, Holt SA. Structural Characterization of a Model Gram-Negative Bacterial Surface Using Lipopolysaccharides from Rough Strains of *Escherichia coli*. Biomacromolecules. 2013; 14:2014–2022. [PubMed: 23617615]

26. Nascimento A, Pontes FJS, Lins RD, Soares TA. Hydration, Ionic Valence and Cross-Linking Propensities of Cations Determine the Stability of Lipopolysaccharide (LPS) Membranes. Chem Commun. 2014; 50:231.

27. Papo N, Shai Y. A Molecular Mechanism for Lipopolysaccharide Protection of Gram-Negative Bacteria from Antimicrobial Peptides. J Biol Chem. 2005; 280:10378–10387. [PubMed: 15632151]

28. Wang X, Quinn PJ. Lipopolysaccharide: Biosynthetic Pathway and Structure Modification. Prog Lipid Res. 2010; 49:97–107. [PubMed: 19815028]

29. Kirschner KN, Lins RD, Maass A, Soares TA. A Glycam-Based Force Field for Simulations of Lipopolysaccharide Membranes: Parametrization and Validation. J Chem Theory Comput. 2012; 8:4719–4731.

30. Nikaido H. Molecular Basis of Bacterial Outer Membrane Permeability Revisited. Microbiol Mol Biol Rev. 2003; 67:593–656. [PubMed: 14665678]

31. Furukawa Y, Dale JR. The Surface Properties of *Shewanella putrefaciens* 200 and *S. oneidensis* MR-1: The Effect of pH and Terminal Electron Acceptors. Geochem Trans. 2013; 14:3. [PubMed: 23566080]

32. Korenevsky AA, Vinogradov E, Gorby Y, Beveridge TJ. Characterization of the Lipopolysaccharides and Capsules of *Shewanella* Spp. Appl Environ Microbiol. 2002; 68:4653–4657. [PubMed: 12200327]

33. Neal AL, Dublin SN, Taylor J, Bates DJ, Burns JL, Apkarian R, DiChristina TJ. Terminal Electron Acceptors Influence the Quantity and Chemical Composition of Capsular Exopolymers Produced by Anaerobically Growing *Shewanella* Spp. Biomacromolecules. 2007; 8:166–174. [PubMed: 17206803]

34. Thill A, Zeyons O, Spalla O, Chauvat F, Rose J, Auffan M, Flank AM. Cytotoxicity of CeO_2 Nanoparticles for *Escherichia coli*. Physico-Chemical Insight of the Cytotoxicity Mechanism. Environ Sci Technol. 2006; 40:6151–6156. [PubMed: 17051814]

35. Sondi I, Salopek-Sondi B. Silver Nanoparticles as Antimicrobial Agent: A Case Study on *E. coli* as a Model for Gram-Negative Bacteria. J Colloid Interface Sci. 2004; 275:177–182. [PubMed: 15158396]

36. Amro NA, Kotra LP, Wadu-Mesthrige K, Bulychev A, Mobashery S, Liu G. High-Resolution Atomic Force Microscopy Studies of the *Escherichia coli* Outer Membrane: Structural Basis for Permeability. Langmuir. 2000; 16:2789–2796.

37. Kotra LP, Golemi D, Amro NA, Liu GY, Mobashery S. Dynamics of the Lipopolysaccharide Assembly on the Surface of *Escherichia coli*. J Am Chem Soc. 1999; 121:8707–8711.

38. Vinogradov E, Korenevsky A, Beveridge TJ. The Structure of the Rough-Type Lipopolysaccharide from *Shewanella oneidensis* MR-1, Containing 8-Amino-8-Deoxy-Kdo and an Open-Chain Form of 2-Acetamido-2-Deoxy-D-Galactose. Carbohydr Res. 2003; 338:1991–1997. [PubMed: 14499575]

39. Gattis SG, Chung HS, Trent MS, Raetz CRH. The Origin of 8-Amino-3,8-Dideoxy-D-Manno-Octulosonic Acid (Kdo8N) in the Lipopolysaccharide of *Shewanella oneidensis*. J Biol Chem. 2013; 288:9216–9225. [PubMed: 23413030]

40. Vetten MA, Tlotleng N, Rascher DT, Skepu A, Keter FK, Boodhia K, Koekemoer LA, Andraos C, Tshikhudo R, Gulumian M. Label-Free in Vitro Toxicity and Uptake Assessment of Citrate Stabilised Gold Nanoparticles in Three Cell Lines. Part Fibre Toxicol. 2013; 10:50. [PubMed: 24103467]
41. Hancock, IC. Microbial Cell Surface Architecture. In: Mozes, N.; Handley, PS.; Busscher, HJ.; Rouxhet, PG., editors. Microbial Cell Surface Analysis. VCH; Weinheim, Germany: 1991. p. 21-59.
42. Brooks, GF.; Carroll, KC.; Butel, JS.; Morse, SA.; Mietzner, TA. Jawetz, Melnick, & Adelberg's Medical Microbiology. McGraw-Hill; USA: 2010.
43. Radovic-Moreno AF, Lu TK, Puscasu VA, Yoon CJ, Langer R, Farokhzad OC. Surface Charge-Switching Polymeric Nanoparticles for Bacterial Cell Wall-Targeted Delivery of Antibiotics. ACS Nano. 2012; 6:4279–4287. [PubMed: 22471841]
44. Feris K, Otto C, Tinker J, Wingett D, Punnoose A, Thurber A, Kongara M, Sabetian M, Quinn B, Hanna C, et al. Electrostatic Interactions Affect Nanoparticle-Mediated Toxicity to Gram-Negative Bacterium *Pseudomonas aeruginosa* PAO1. Langmuir. 2010; 26:4429–4436. [PubMed: 20000362]
45. Strain SM, Armitage IM. Selective Detection of 3-Deoxymannooctulosonic Acid in Intact Lipopolysaccharides by Spin-Echo 13C NMR. J Biol Chem. 1985; 260:12974–12977. [PubMed: 3902810]
46. Raetz CRH, Whitfield C. Lipopolysaccharide Endotoxins. Annu Rev Biochem. 2002; 71:635–700. [PubMed: 12045108]
47. Chng SS, Ruiz N, Chimalakonda G, Silhavy TJ, Kahne D. Characterization of the Two-Protein Complex in *Escherichia coli* Responsible for Lipopolysaccharide Assembly at the Outer Membrane. Proc Natl Acad Sci U S A. 2010; 107:5363–5368. [PubMed: 20203010]
48. Dumitriu, S. Polysaccharides: Structural Diversity and Functional Versatility. CRC Press; Hoboken, NJ: 1998.
49. Strauss J, Burnham NA, Camesano TA. Atomic Force Microscopy Study of the Role of LPS O-Antigen on Adhesion of *E. coli*. J Mol Recognit. 2009; 22:347–355. [PubMed: 19402104]
50. Beveridge TJ, Graham LL. Surface Layers of Bacteria. Microbiol Molecularbiol Rev. 1991; 55:684–705.
51. Soares TA, Straatsma TP, Lins RD. Influence of the B-Band O-Antigen Chain in the Structure and Electrostatics of the Lipopolysaccharide Membrane of *Pseudomonas aeruginosa*. J Braz Chem Soc. 2008; 19:312–320.
52. Troiano JM, Olenick LL, Kuech TR, Melby ES, Hu D, Lohse SE, Mensch AC, Doğangün M, Vartanian AM, Torelli M, Ehimiaghe E, Walter SR, Fu L, Wang F, Orr G, Murphy CJ, Hamers RJ, Pedersen JA, Geiger FM. Direct probes of 4-nm diameter gold nanoparticles interacting with supported lipid bilayers. J Phys Chem C. 2015; 119:534–546.
53. Steel WH, Walker RA. Measuring Dipolar Width across Liquid-Liquid Interfaces with "Molecular Rulers. Nature. 2003; 424:296–299. [PubMed: 12867977]
54. Steel WH, Damkaci F, Nolan R, Walker RA. Molecular Rulers: New Families of Molecules for Measuring Interfacial Widths. J Am Chem Soc. 2002; 124:4824–4831. [PubMed: 11971732]
55. Liu P, Kendelewicz T, Nelson EJ, Brown GE. Reaction of Water with MgO(100) Surfaces: Part III. X-Ray Standing Wave Studies. Surf Sci. 1998; 415:156–169.
56. Eckhardt S, Brunetto PS, Gagnon J, Priebe M, Giese B, Fromm KM. Nanobio Silver. Its Interactions with Peptides and Bacteria, and Its Uses in Medicine. Chem Rev. 2013; 113:4708–4754. [PubMed: 23488929]
57. Xia T, Kovochich M, Liong M, Mädler L, Gilbert B, Shi H, Yeh JI, Zink JI, Nel AE. Comparison of the Mechanism of Toxicity of Zinc Oxide and Cerium Oxide Nanoparticles Based on Dissolution and Oxidative Stress Properties. ACS Nano. 2008; 2:2121–2134. [PubMed: 19206459]

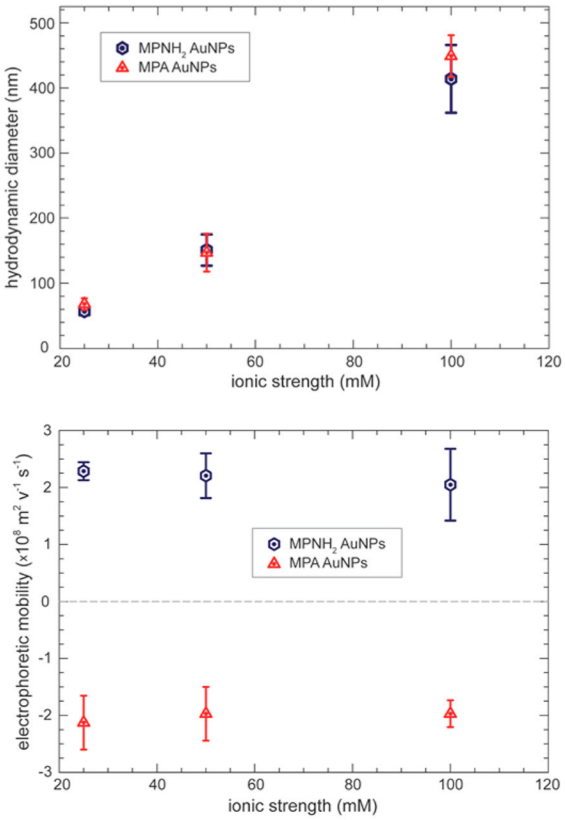

Figure 1.

(a) Number-average hydrodynamic diameters and (b) electrophoretic mobilities of MPA- and $MPNH_2$-functionalized gold nanoparticles (AuNPs) as a function of solution ionic strength. All values were measured at a (particle number) concentration of 12.8 nM in 2 mM HEPES solution (pH 7.4). The desired ionic strength was achieved by the addition of NaCl. Error bars represent one standard deviation (n = 10).

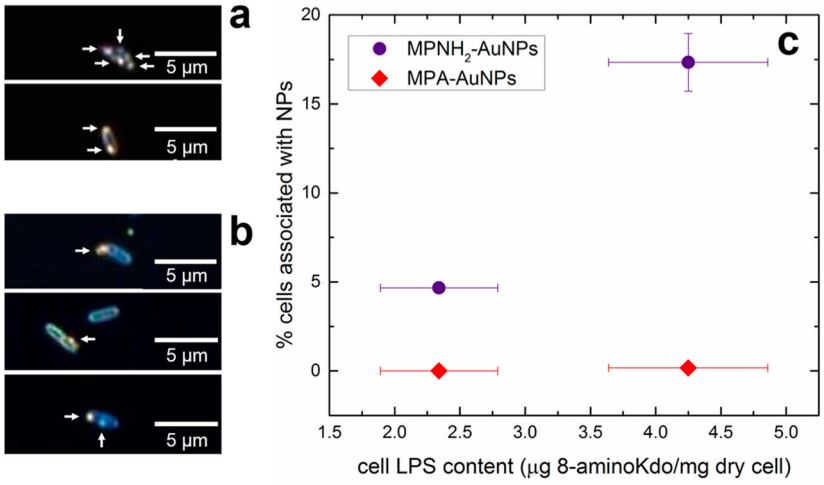

Figure 2.

Gold nanoparticle association with bacterial cells is directly observable and depends on cell LPS content. (a) Cells isolated (sorted) from the total cell population after exposure to $MPNH_2$-AuNPs. (b) Unsorted cells after exposure to $MPNH_2$-AuNPs. In panels a and b the arrows point to AuNPs associated with the cells as confirmed by hyperspectral imaging. (c) Association of MPA- or $MPNH_2$-AuNPs with *Shewanella* cells with varying LPS content (indicated by 8-amino-2-keto-3-deoxy-D-manno-octonate (8-aminoKdo) content of lyophilized cells) quantified by flow cytometry. Error bars (representing one standard deviation, $n = 3$) are smaller than the symbol in some cases.

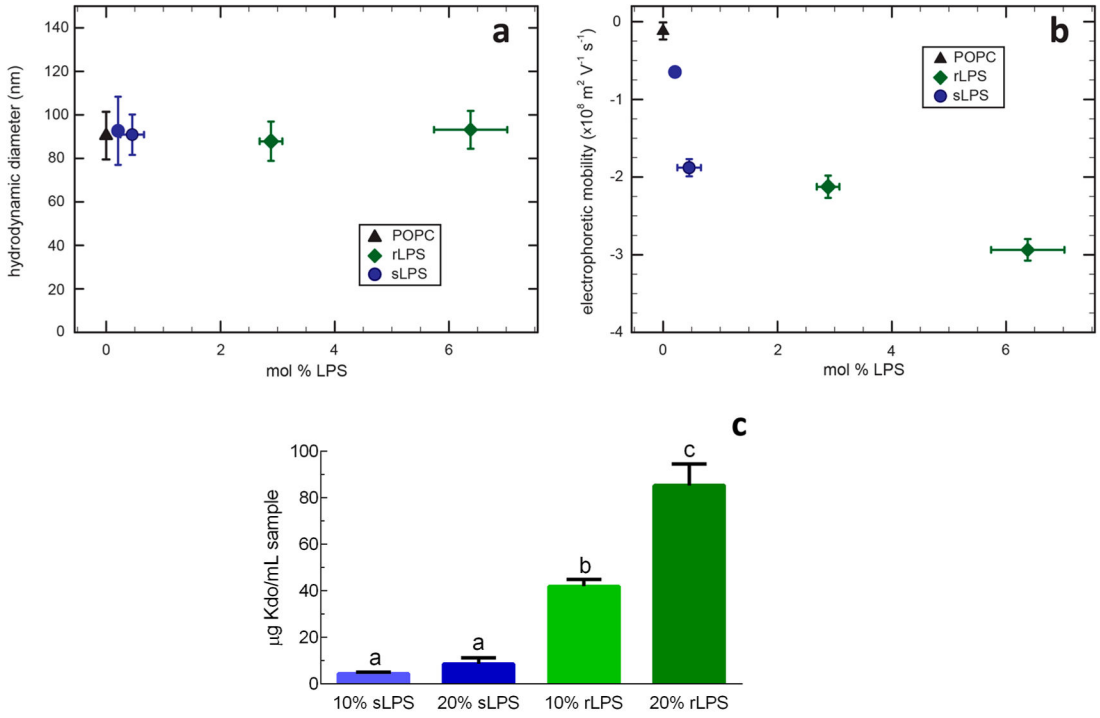

Figure 3.

(a) Hydrodynamic diameters and (b) electrophoretic mobilities of unilamellar vesicles composed of POPC or POPC and the indicated mole percent of either smooth LPS (sLPS) or rough LPS (rLPS). Apparent ζ potentials derived from these electrophoretic mobility measurements are presented in Figure S7. All values were measured at a vesicle concentration of 10 $\mu g \cdot mL^{-1}$ in a 0.002 M HEPES (pH 7.4), 0.001 M NaCl solution. Error bars represent one standard deviation ($n = 5$). (c) Content of 2-keto-3-deoxy-D-manno-octonate (Kdo) in the POPC/LPS vesicles as a function of mass percent LPS addition (used to estimate mol % LPS in vesicles). Each smooth LPS molecule contains three Kdo residues while each rough LPS molecule contains two Kdo residues.[45,46] Error bars represent one standard deviation ($n = 3$). Values labeled with different letters differ significantly from each other ($p < 0.05$).

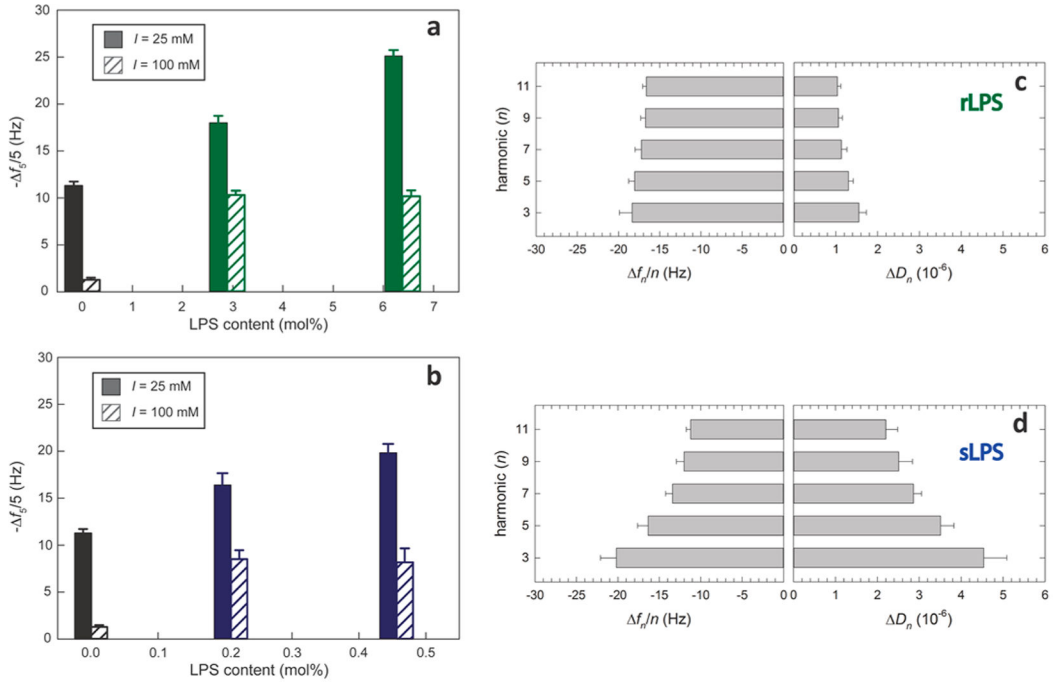

Figure 4.

Association of $MPNH_2$-AuNPs with bilayers containing (a) rough or (b) smooth LPS. Normalized maximum frequency shifts for the 5th harmonic ($\Delta f_5/5$) during nanoparticle-bilayer exposure are displayed. Calculation of mole percent LPS content assumed three Kdo molecules per smooth LPS molecule and two Kdo molecules per smooth LPS molecule.[45,46] Error bars represent one standard deviation (n = 3). (c,d) The harmonic-dependence of Δf_n and the energy dissipation factor (ΔD_n), where n is the harmonic number, is more pronounced for $MPNH_2$-AuNPs interacting with bilayers containing rough LPS (panel c) than smooth LPS (panel d).[19] Experiments were performed in 0.002 M HEPES (pH 7.4) and 0.025 M NaCl.

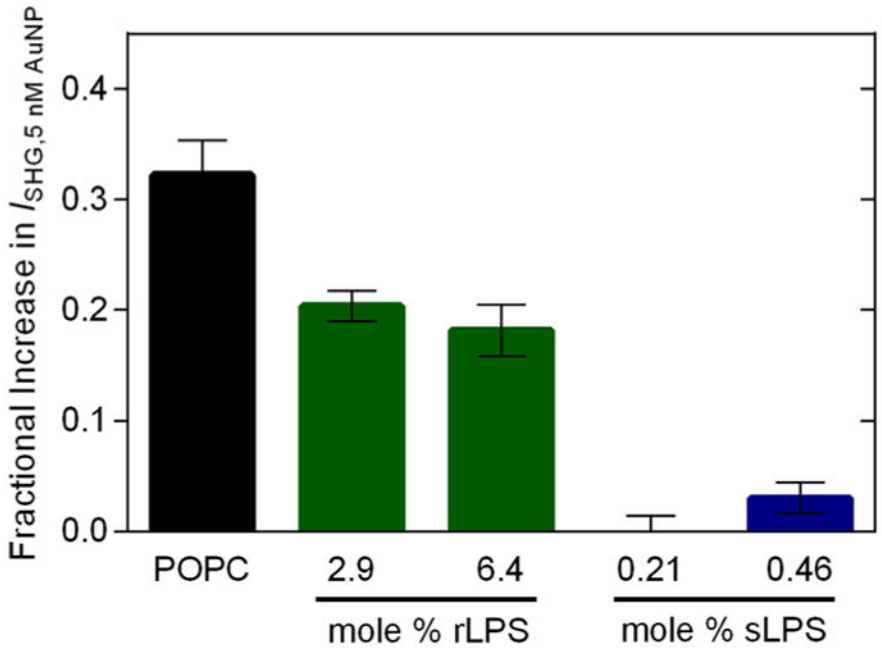

Figure 5.

Observed changes in SHG signal intensity following introduction of $MPNH_2$-AuNPs (5×10^{-9} M number density) to POPC bilayers lacking LPS (black), or containing rough LPS (rLPS, green) or smooth LPS (sLPS, blue). The observed SHG signal arises from nanoparticle-induced resonance enhancement near the bilayer–solution interface. All experiments were performed in 0.002 M HEPES (pH 7.4) and 0.025 M NaCl.